AD-A043 610 INCOSYM INC CALABASAS CA F/G 17/7
INCOFLEX TWO AXES ACCELEROMETER PROGRAM.(U)
AUG 77 J RUSSELL, R J CRAIG DAAK40-76-C-1025

UNCLASSIFIED NL

| OF |
AD
A043 610

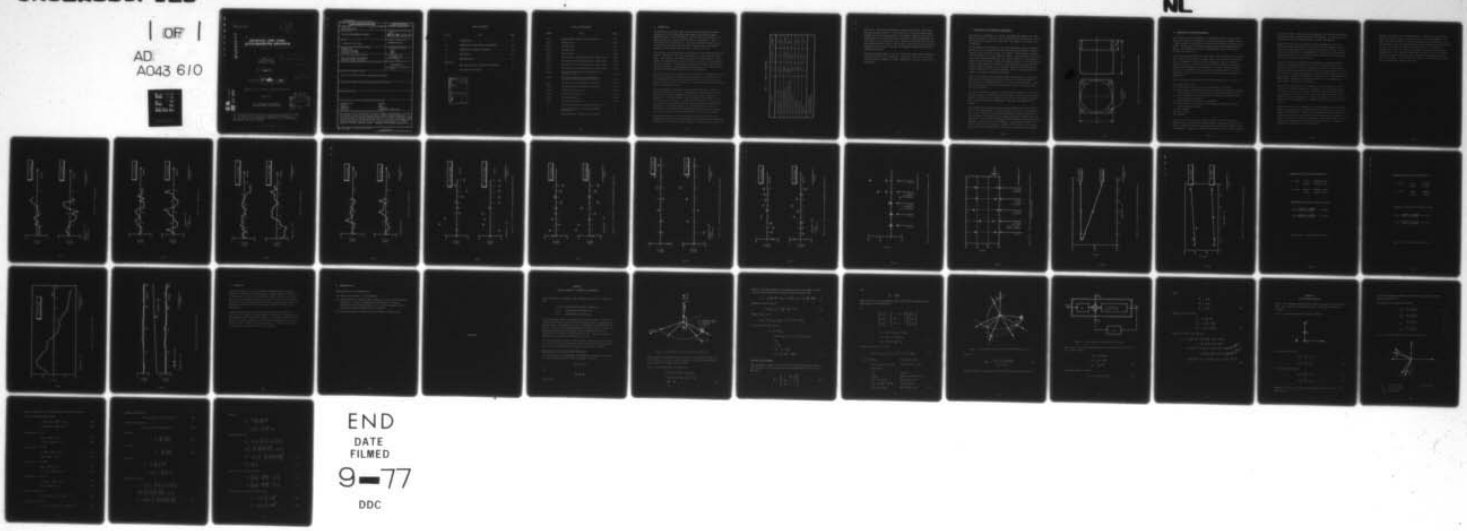

END
DATE
FILMED
9-77
DDC

(15) DAAK40-76-C-1025

(12) B.S.

(6) INCOFLEX TWO AXES ACCELEROMETER PROGRAM

(10) J. Russell
R. J. Craig

INCOSYM, INC.
23931 Ventura Blvd.
Calabasas, CA 91302

(11) August 1977

(12) 43 p.

(9) FINAL REPORT
Period 22 June 1976 through 26 July 1977

Approved For Public Release, Distribution Unlimited

Prepared For

U.S. ARMY MISSILE R&D COMMAND
REDSTONE ARSENAL, ALABAMA 35809

The views and conclusions contained in this document are those of Incosym, Inc., and should not be interpreted as necessarily representing the official policies, either expressed or implied, of the U.S. Army Missile R&D Command or the U.S. Government.

Unclassified

SECURITY CLASSIFICATION OF THIS PAGE *(When Data Entered)*

REPORT DOCUMENTATION PAGE		READ INSTRUCTIONS BEFORE COMPLETING FORM
1. REPORT NUMBER DAAK40-76-C-1025	2. GOVT ACCESSION NO.	3. RECIPIENT'S CATALOG NUMBER
4. TITLE *(and Subtitle)* Incoflex Accelerometer Program		5. TYPE OF REPORT & PERIOD COVERED Final 22 June 1976 - 26 July 1977 6. PERFORMING ORG. REPORT NUMBER
7. AUTHOR(s) J. Russell, R.J. Craig		8. CONTRACT OR GRANT NUMBER(s) DAAK40-76-C-1025
9. PERFORMING ORGANIZATION NAME AND ADDRESS INCOSYM, Inc 23931 Ventura Blvd Calabasas, Ca 91302		10. PROGRAM ELEMENT, PROJECT, TASK AREA & WORK UNIT NUMBERS A100 A780
11. CONTROLLING OFFICE NAME AND ADDRESS U.S. Army Missile R&D Command Redstone Arsenal, Al 35809		12. REPORT DATE 16 August 1977 13. NUMBER OF PAGES 41
14. MONITORING AGENCY NAME & ADDRESS*(if different from Controlling Office)*		15. SECURITY CLASS. *(of this report)* Unclassified 15a. DECLASSIFICATION/DOWNGRADING SCHEDULE

16. DISTRIBUTION STATEMENT *(of this Report)*

Approved for public release, distribution unlimited

17. DISTRIBUTION STATEMENT *(of the abstract entered in Block 20, if different from Report)*

18. SUPPLEMENTARY NOTES

19. KEY WORDS *(Continue on reverse side if necessary and identify by block number)*

Accelerometer	Torquer
Flexure	Bias
Suspension	Stability
Pendulous	Temperature Sensitivity

20. ABSTRACT *(Continue on reverse side if necessary and identify by block number)*

The purpose of the contract was to build 2 two-axes accelerometers, test them and deliver to the U.S. Army Missile Command. These accelerometers were to be accurate enough for inertial navigation but were to require no heating or thermal control. This report documents the effort and the test results. The performance demonstrated indicates that the Incoflex accelerometer is a viable candidate for fast reaction, accurate navigation and guidance applications.

DD FORM 1 JAN 73 1473 EDITION OF 1 NOV 65 IS OBSOLETE

Unclassified

SECURITY CLASSIFICATION OF THIS PAGE *(When Data Entered)*

TABLE OF CONTENTS

LIST OF ILLUSTRATIONS

I INTRODUCTION

The following is the final report on the two axis accelerometer program sponsored by the U.S. Army Missile R&D Command under contract number DAAK40-76-C-1025. The work performed under the contract consisted of the design, fabrication, test and delivery of two accelerometers. These accelerometers are unfloated, i.e., contain no floatation fluids, and each can measure acceleration along two axes at the same time. The program spanned a twelve month period from July of 1976 to July 1977.

The objective of the program was to utilize previous knowledge and experience gained by INCOSYM Inc. during the development of a tuned suspension gyroscope. This knowledge and experience consisted of observations of the performance of component parts of the gyroscope, and their fabrication methods and test techniques. It had appeared from testing of these component parts and from the resultant Incoflex gyro performance, that with correct modification the technology would be applicable to accelerometers.

The major incentive from an applications viewpoint was the possibility, based on the gyro experience, of producing a very accurate accelerometer with a low bias temperature sensitivity, and that had two sensing axes that were fabricated and tested as one single unit. This has the appeal of getting two axes for the same price as one.

The bias temperature sensitivity of accelerometers has been a problem in applications requiring accuracy. The temperature sensitivity has typically been of an unacceptable magnitude and non-linear, making compensation impractical. Therefore, systems had to be thermally controlled, and the reaction time of the system, i.e., the time from turn-on to firing or take-off, was long due to having to wait for heating and thermal stabilization. Consequently a design was produced, two accelerometers were built and delivered to the U.S. Army Missile R&D Command. Torquing loop electronics were also designed and fabricated and delivered with the accelerometers.

An analytical prediction of the performance had been made, so the test sequence was designed to evaluate the actual versus the predicted performance. A synopsis of the results are shown in Table I. The detailed test data is in

TABLE I-1. SUMMARY OF PERFORMANCE

Parameter	Units	Goal Spec.	Measured
Bias Stability - Long Term	μg 1σ	40	100
Bias Stability - One Hour	μg 1σ	2.5	2.5
Bias Temperature Sensitivity	$\mu g/^{O}F$	0.25*	0.3**
Scale Factor Temperature Coefficient	PPM/^{O}F	<250	230
Scale Factor Stability	PPM	<10	-
Axis Alignment	mrad	0.3	0.03
Reaction Time	sec	<10	3
Bandwidth	Hz	>10	165

*With Compensation
**Without Compensation

Section III. The actual performance met the predicted in all cases except the long term bias stability. It was difficult to correctly evaluate this parameter due to the short duration of the program. However, the tests performed indicated a value that would be acceptable for many applications, but that did not meet the predicted value. Further consideration indicated that the predicted value is correct, and also that a modification in the design and fabrication would result in the long term stability meeting the 40 μg value estimated by analysis.

The most significant aspect of the test results was that the bias temperature sensitivity is very low, as predicted. This and the other data led to the conclusion that the design is a viable candidate for accurate, fast reaction requirements.

II DESCRIPTION OF THE INCOFLEX ACCELEROMETER

The Incoflex accelerometer is a two axes, pendulous mass design of the size shown in Figure II-1. The size shown contains both axes but does not include the torquing loop electronics at this time. The weight of the present unit is 200 grams.

The mechanization is as follows. A two axes suspension carries the torquer, which consists of the magnets and flux return path that establish a radially orienated field within the air gap. The torquer is made pendulous relative to both torsional axes of the suspension system. In the presence of accelerations along any axis perpendicular to the axis of symmetry of the suspension system, the pendulous mass is deflected angularly relative to the accelerometer housing. This deflection is sensed by the pickoffs whose output drives the current through the torquer coils, exerting a moment on the pendulous mass in such a direction as to null the pickoffs. Thus the current through the torquer is a measure of applied acceleration.

There are two pickoffs per axis placed diametrically opposite to each other, connected in series opposition so that to the first order the pickoff is only sensitive to the angular motion of the torquer flux return path. There are also two torquer coils per axis connected in such a way so that their affects are additive.

The two axes suspension system is a slightly modified version of that used in the Incoflex gyro. It uses flexures for each axis. The entire two axes suspension is fabricated as a single unit and is made of maraging steel, which has a yield stress point of 290,000 psi. This makes the suspension very durable.

The torquing loop electronics used in this program with the Incoflex accelerometer is an analog design. The pickoff input is a 54K Hz 2.5 volt RMS sine wave. This is modulated by the pickoff secondary to indicate the position of the proof mass. The output from the pickoff secondary is amplified and then demodulated. The resultant DC voltage is passed through an amplification stage that also controls the servo loop bandwidth. The last stage applies either positive or negative DC current, as required by the direction of the input acceleration, to the torquer coils. The output is scaled across a resistor.

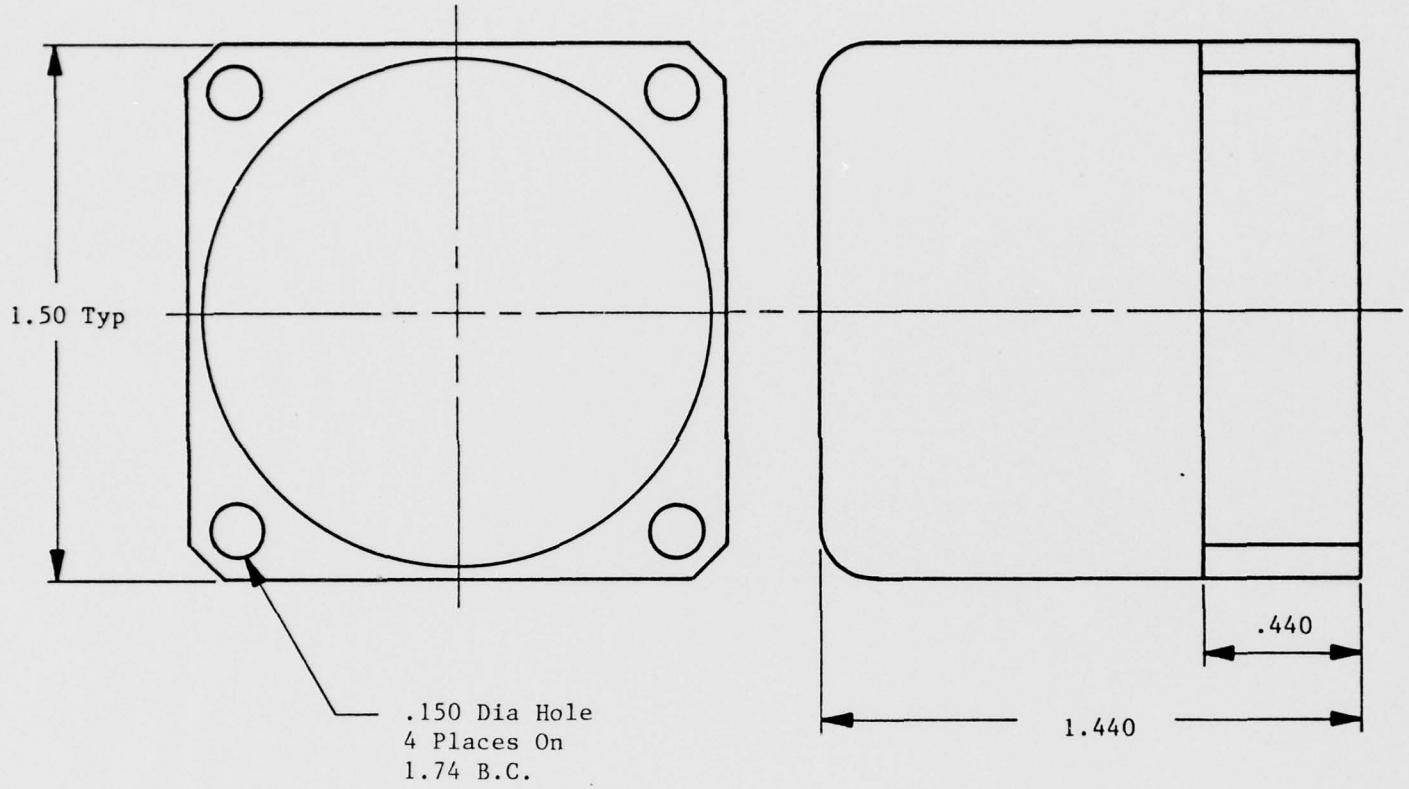

Figure II-1. Accelerometer Outline and Mounting Sketch

III DESCRIPTION OF TESTING AND RESULTS

As the output of the accelerometer is a DC voltage scaled for one (1) volt per g, the readout for testing was a precision differential voltmeter driving a chart recorder. Because this is a two axis accelerometer, two channels were needed. Consequently, two identical Hewlett Packard 3420 Differential Voltmeters, each driving one axis of a two axes Hewlett Packard 7130 A chart recorder, were utilized.

The accelerometer was mounted on a base plate that was fastened into a granite cube. The cube was placed on a granite table. As the faces of the cube are flat and orthogonal to each other, the accelerometer could be tested by rotating the cube on to each of its faces, therefore precisely changing the gravity vector applied to the accelerometer. The data reduction equations are shown in the Appendix. The base plate had heaters installed so that temperature affects on the accelerometer could be measured by increasing the temperature.

The following tests were performed on both accelerometers (No. 1 and No. 2):

(1) Torquer scale factor
(2) Uncompensated torquer scale factor temperature coefficients
(3) Bias stability (drift) during continuous operation for periods of approximately 40 minutes with the pendulous axes both horizontal and vertical.
(4) Bias repeatability over short periods of time with the pendulous axes both horizontal and vertical
(5) Uncompensated bias temperature coefficients
(6) Bias repeatability over several days with some temperature extremes applied between operations
(7) Axis alignment
(8) Reaction time
(9) Bandwidth

The summary of these results is shown in Table I-I in the Introduction. Specific data is shown in the following figures. Figures III-1 and III-2 are the bias stability (drift) with the pendulous axis horizontal (PAH) for each accelerometer. Figures III-3 and III-4 are equivalent runs with the pendulous

axis vertical (PAV). Data on both accelerometers for either PAH and PAV were very similar, and performance was better than expected. No sensitivity to the orientation of the axes was discernable in either accelerometer.

Figures III-5 and III-6 are the short term bias repeatability for each accelerometer with the pendulous axis vertical (PAV) and Figures III-7 and III-8 are the same tests with the pendulous axes horizontal (PAH). All test results were satisfactory. Accelerometer No. 2 showed better repeatability in the PAV position than in the PAH position on both axes, but the data was considered acceptable in either position.

The data for the longer term day-to-day repeatability (Figures III-9 and III-10) are somewhat inconclusive because the test station could not be dedicated to day-to-day testing. Consequently, temperature cycling and re-mounting affects are included in with the day-to-day repeatability. The overall data was not as good as predicted but was encouraging, especially due to the extraneous variables, and would be acceptable for many, and probably most, applications. Further work is anticipated on the next accelerometers to better define and improve the performance.

Figures III-11 and III-12 are very significant in that they show the bias temperature coefficients without any compensation. As the figures show, in all cases this parameter was linear, meaning it could be compensated easily if required, and in three of the four axes, the number is very low. The fourth axis (X on accelerometer No. 1) had a much larger coefficient than the others, and is not considered to be typical of what can be expected in the future.

Torquer scale factors were measured for both accelerometers for information only, as this parameter can be scaled to suit the application. The data is in Figures III-13 and III-14. However, the uncompensated torquer scale factor temperature coefficient was also tested and is shown in the same figures. The number that resulted was exactly as predicted for the magnet material used, and would be compensated for most applications when no heat is applied to stabilize the temperature of the accelerometer.

Two extra tests were run on accelerometer No. 2. These were a bias stability (drift) test over 15 hours and a bias stability test over four minutes. The first test (shown in Figure III-15) was to ascertain the performance when the accelerometer is used in a system that would remain operating over long periods of time. The second test (shown in Figure III-16) was to evaluate the performance when used in a system that required accelerometer stabilization to gyrocompass. The 3 μg/minute slope shown in Figure III-16 is the maximum bias drift acceptable if the system were required to gyrocompass to within one (1) milliradian. As can be seen in the figure, the performance was judged to be well within the required bias drift.

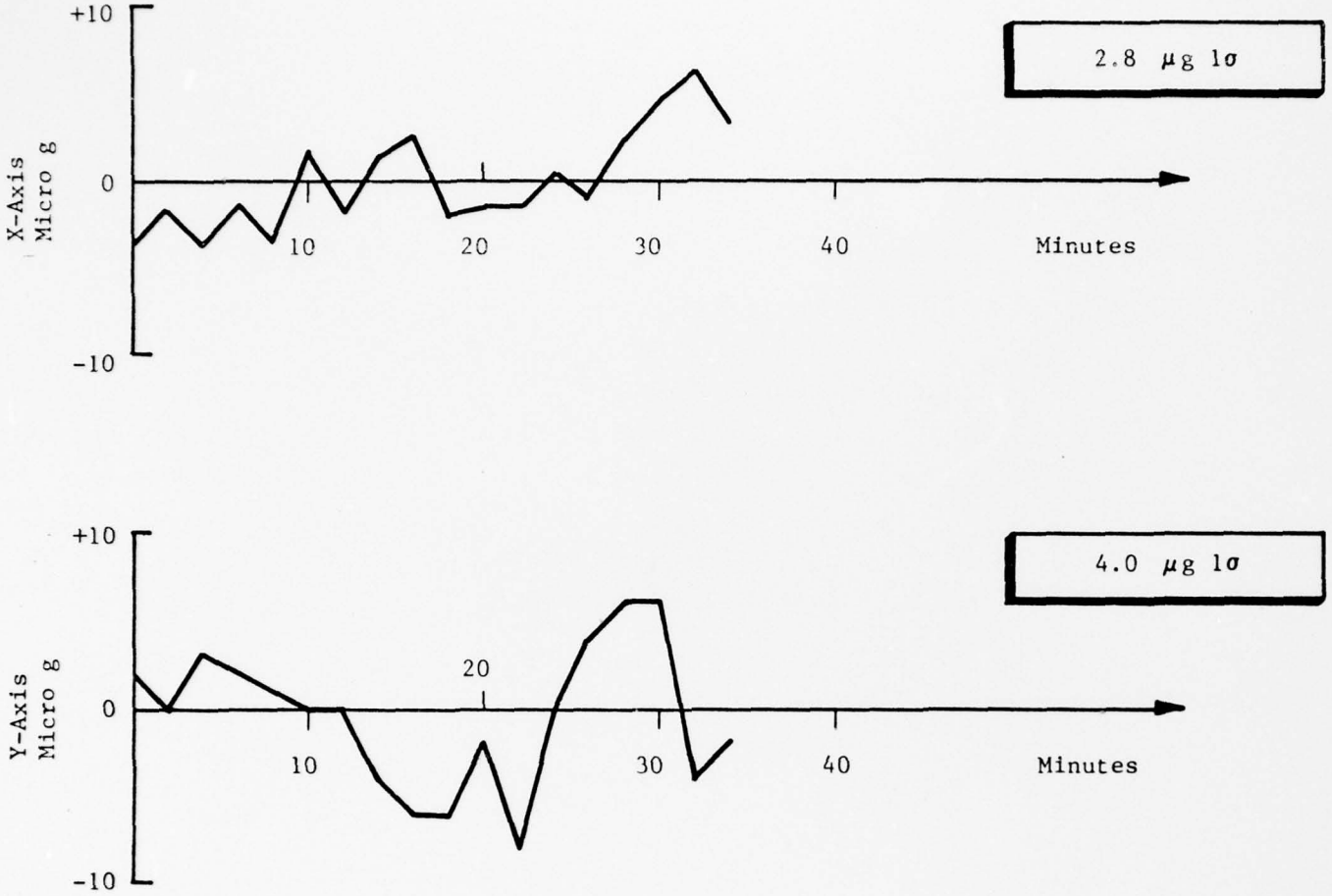

Temperature; 26°C
X_T Down
Y_T Carries 1g

Accelerometer No. 1
8-5-77

Figure III-1. PAH Drift Run

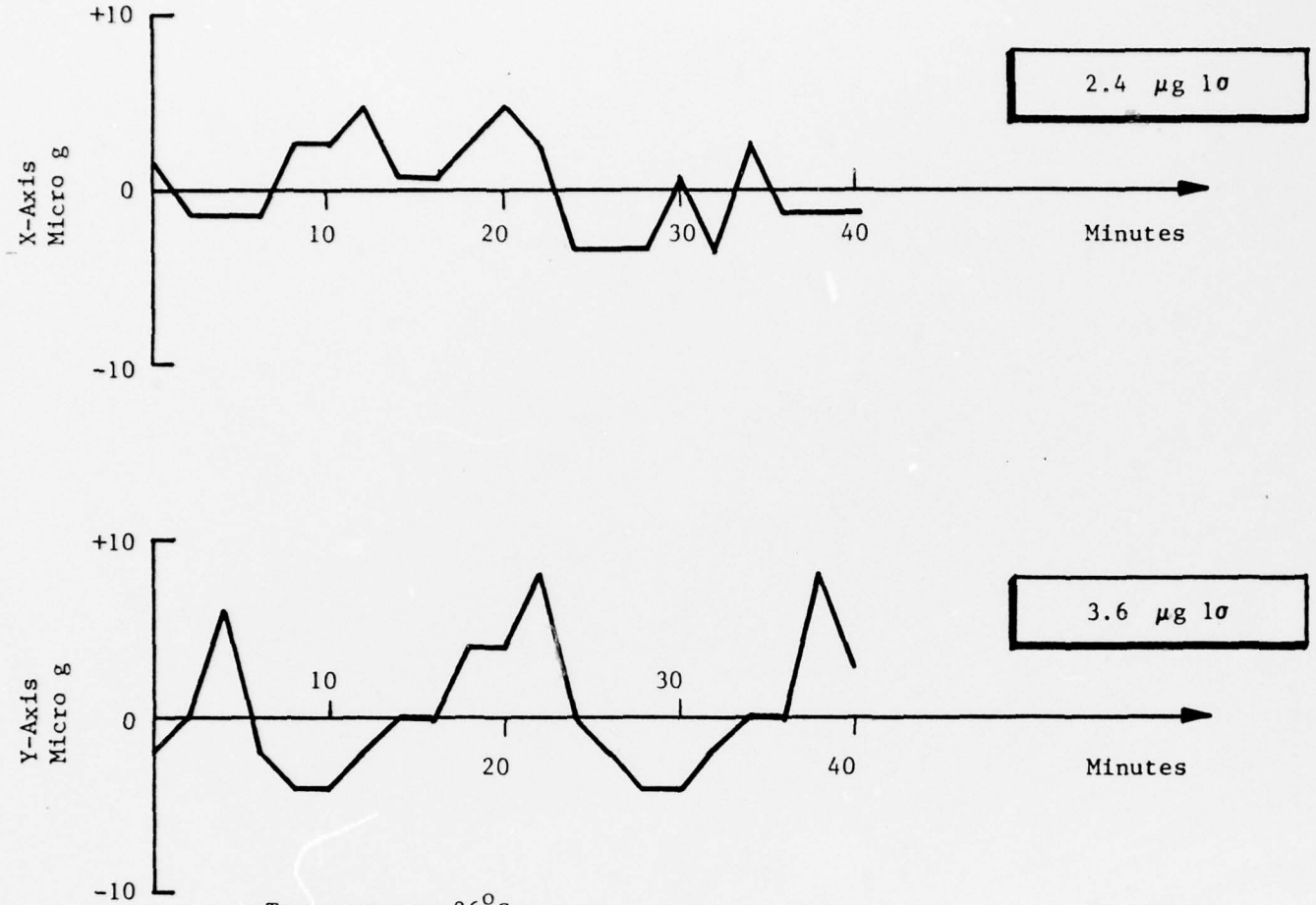

Figure III-2. PAH Drift Run

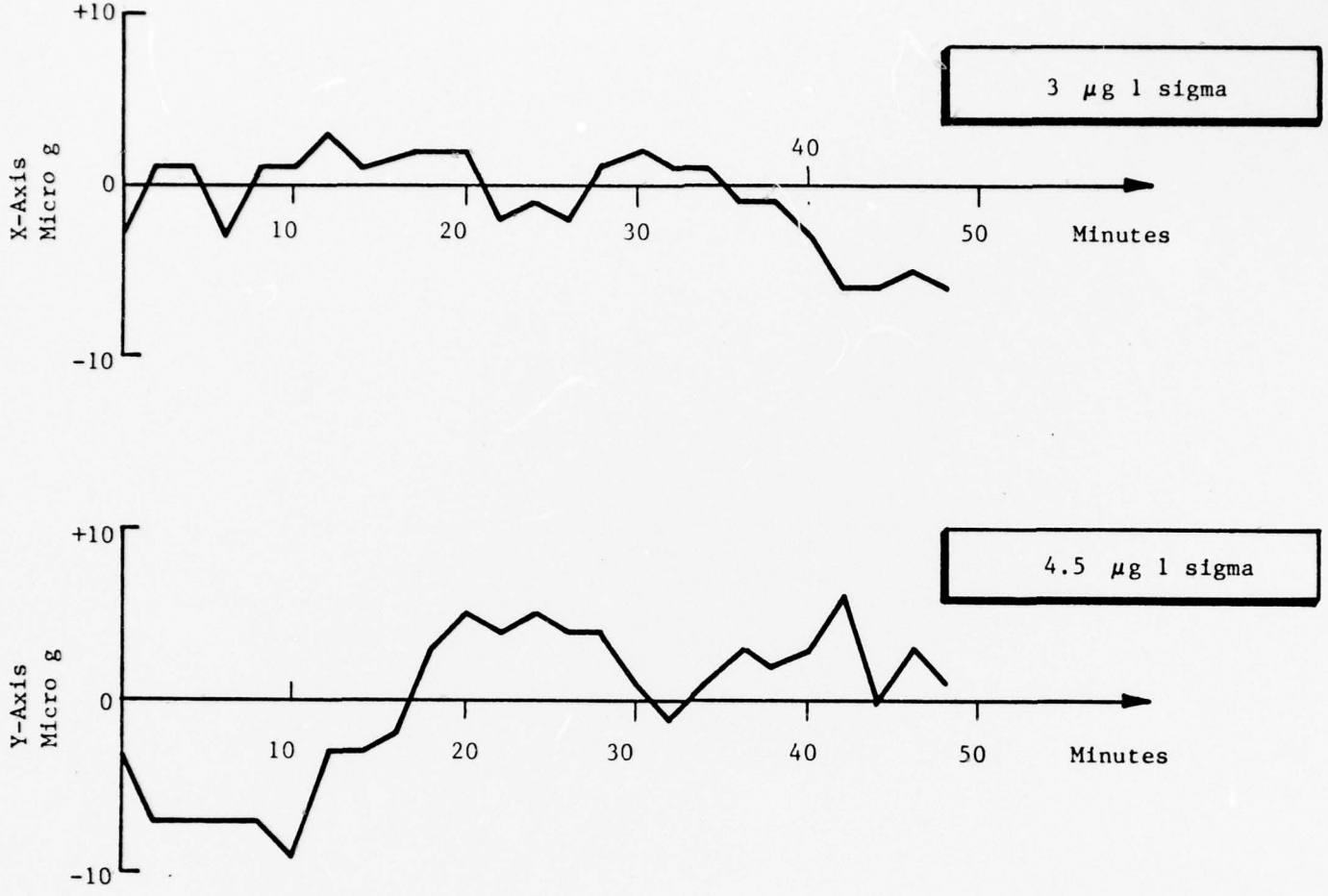

Figure III-3. PAV Drift Run

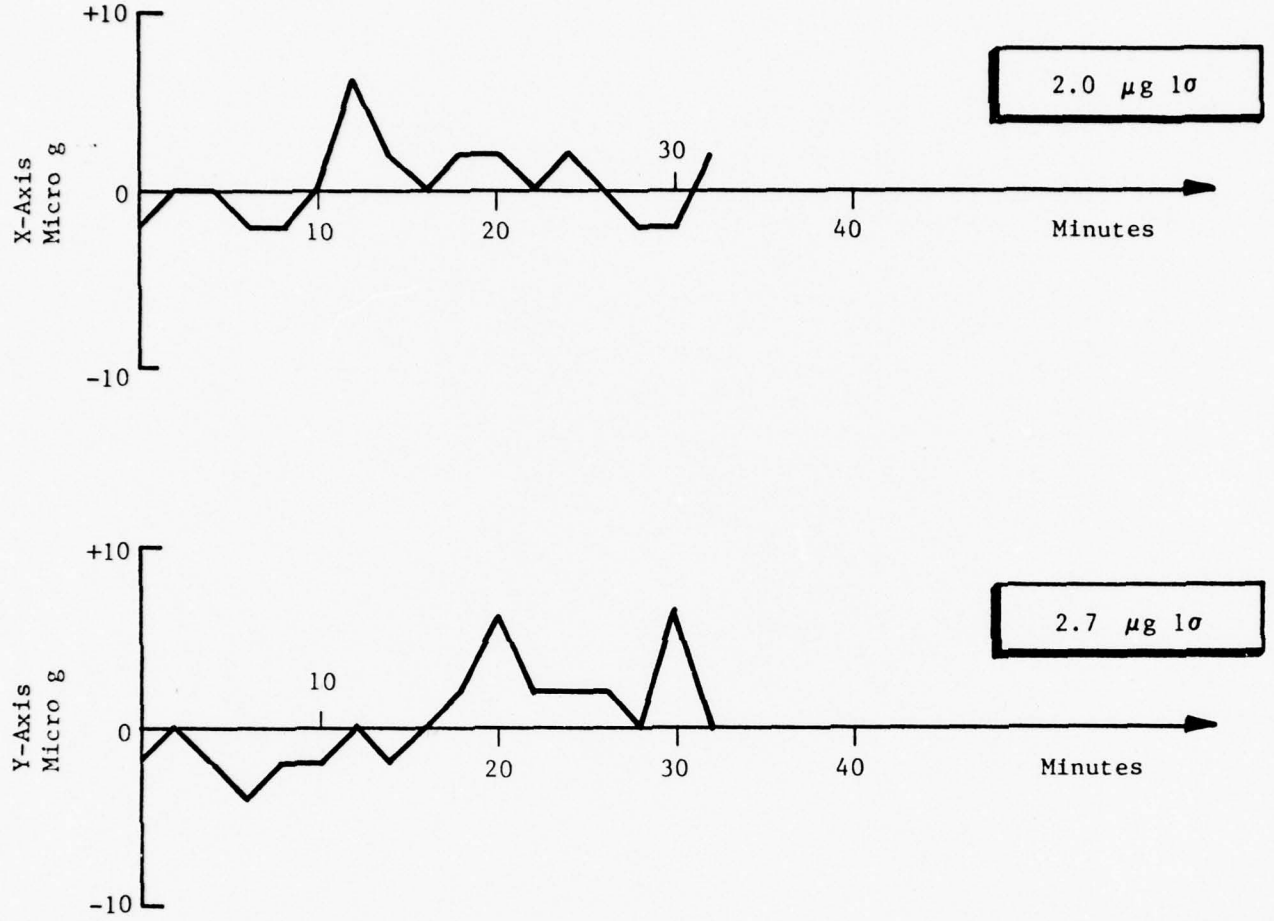

Figure III-4. PAV Drift Run

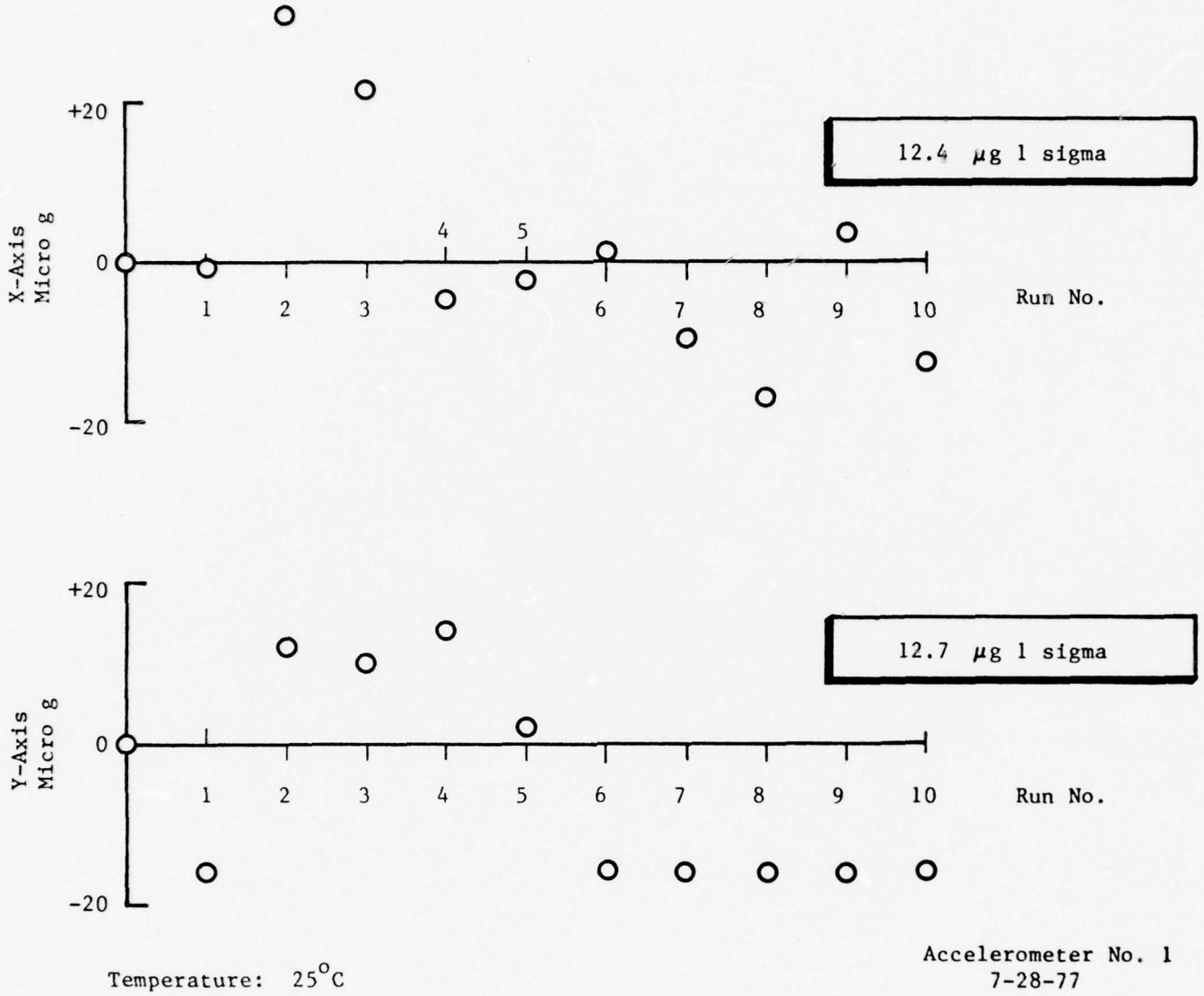

Figure III-5. PAV Turn-On to Turn-On Repeatability (Short Term)

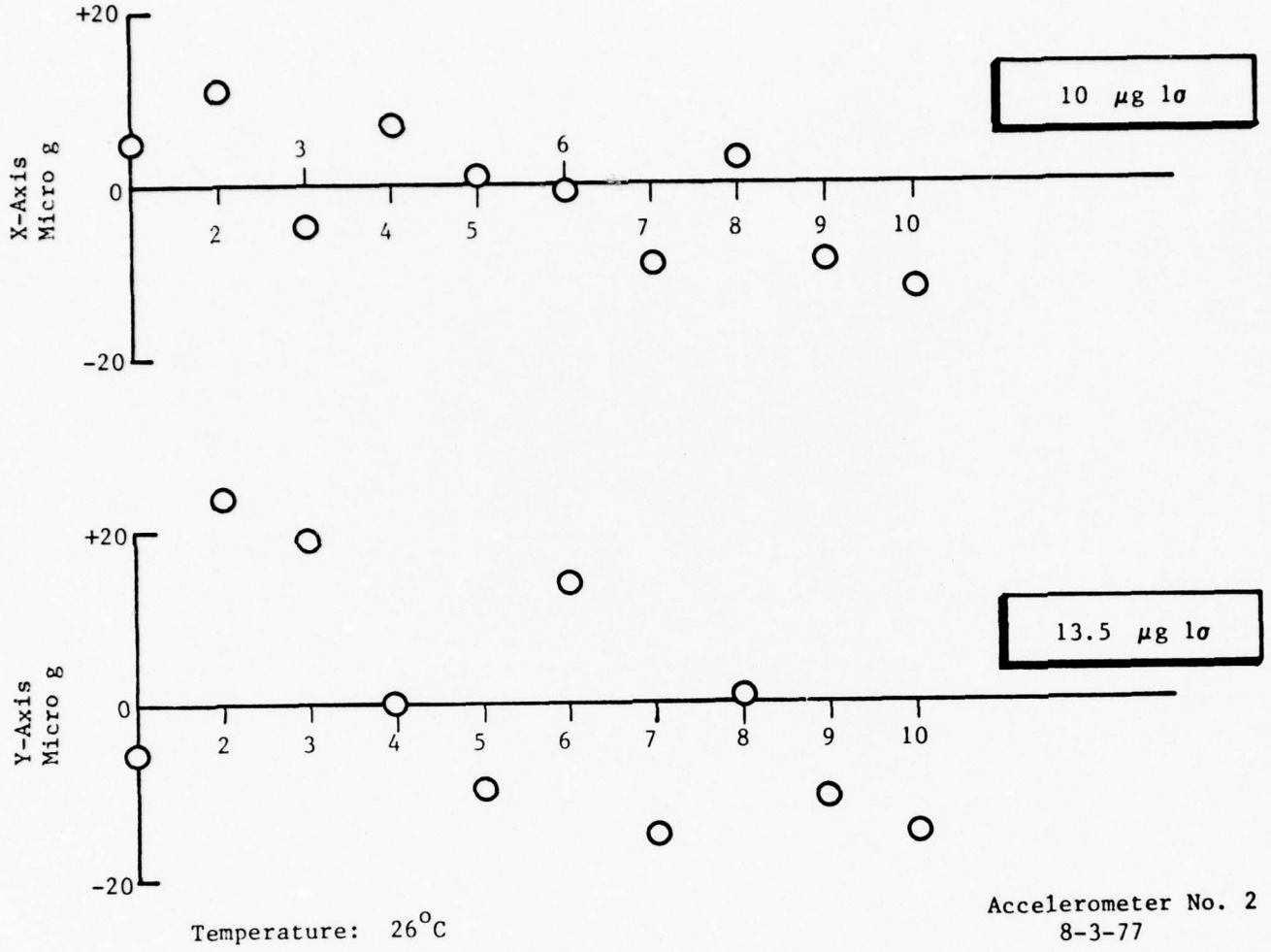

Figure III-6. PAV Turn-On to Turn-On Repeatability (Short Term)

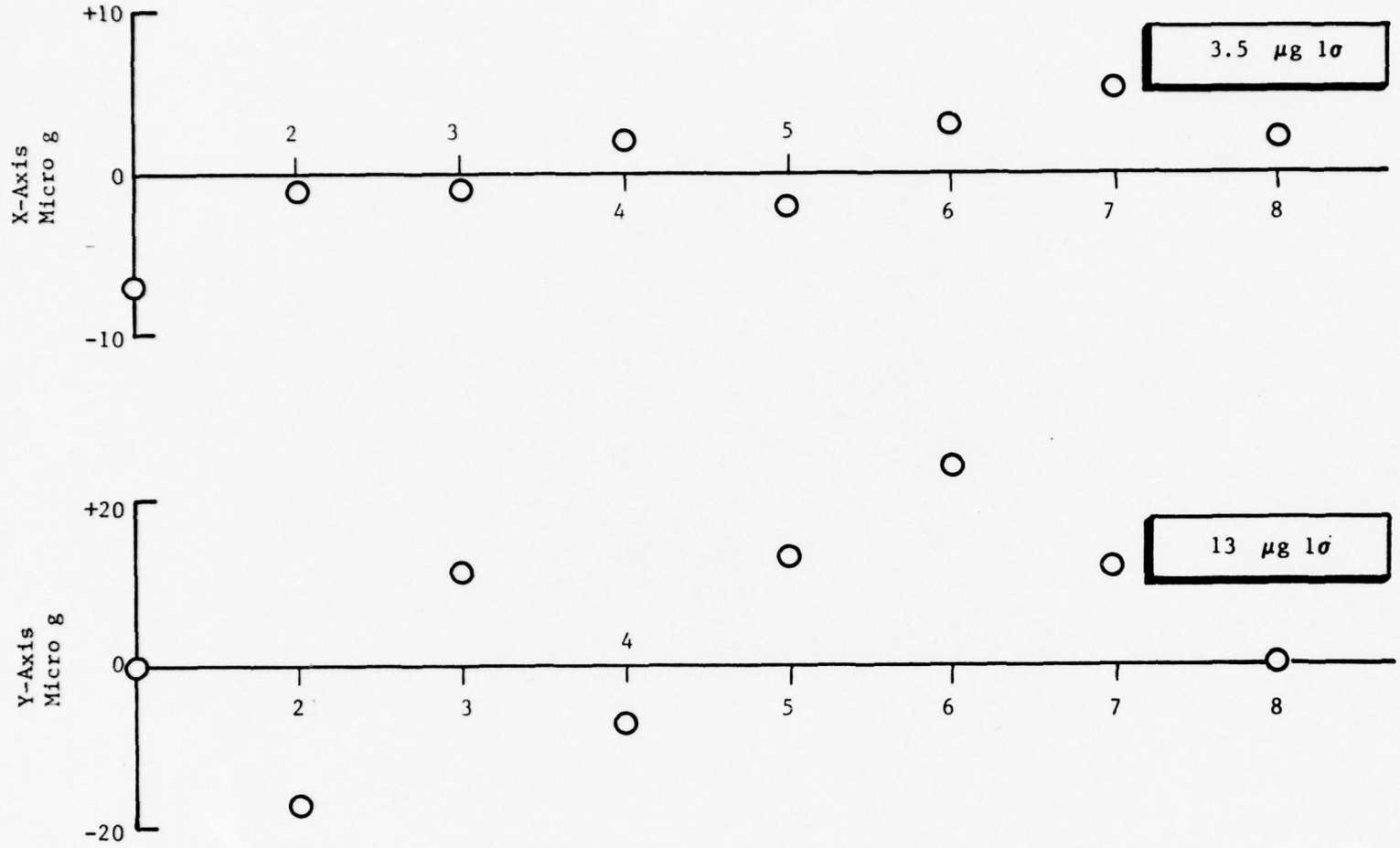

Temperature; 26°C
X Down
Y Carries 1g

Accelerometer No. 1
8-4-77

Figure III-7. PAH Turn-On to Turn-On Repeatability (Short Term)

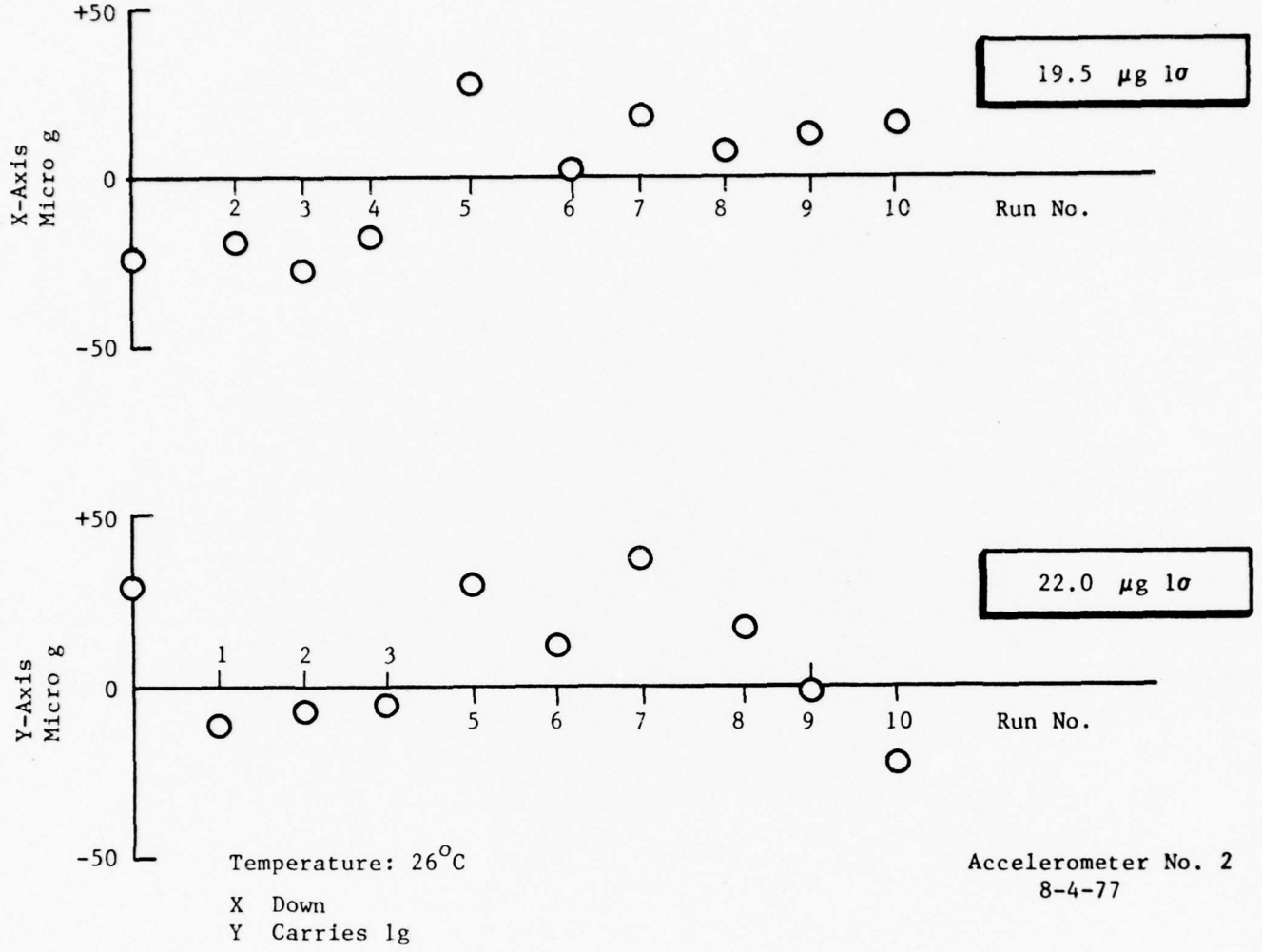

Figure III-8. PAH Turn-On to Turn-On Repeatability (Short Term)

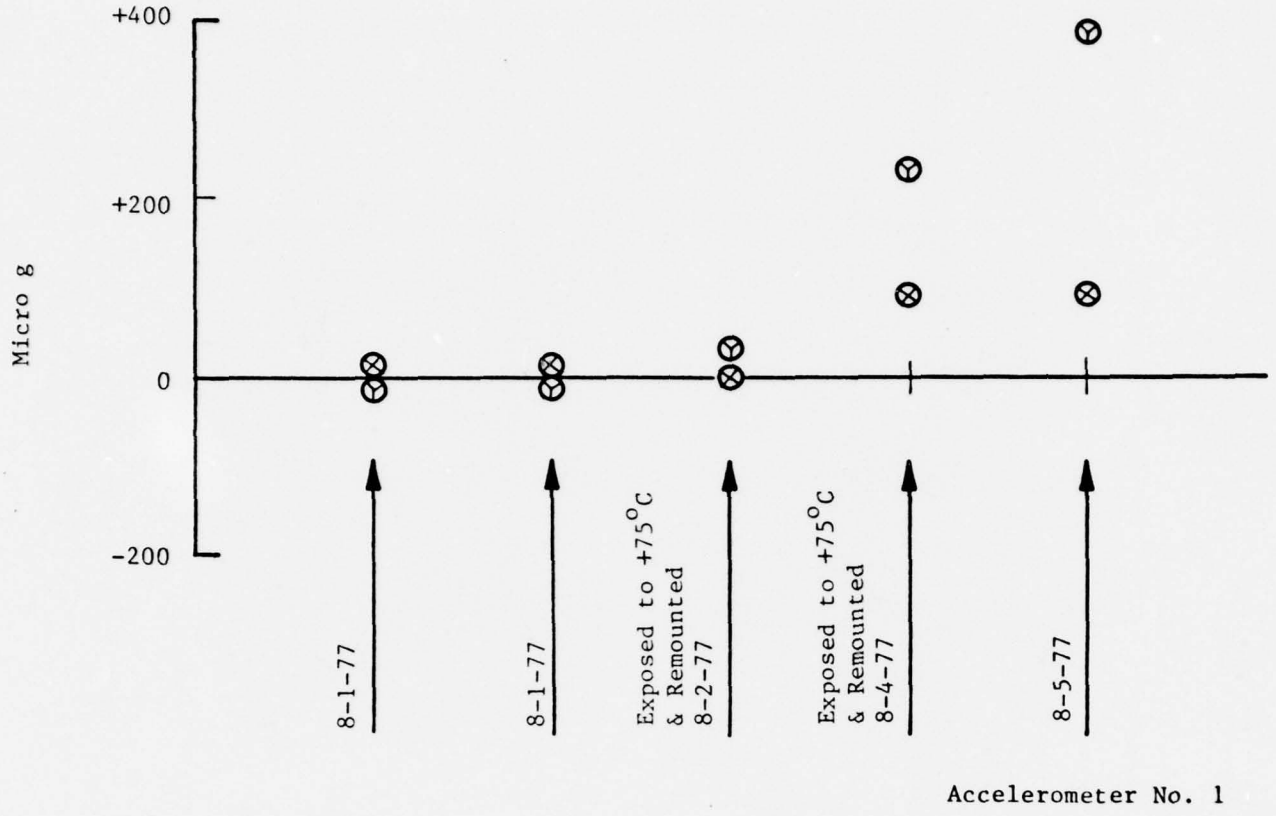

Figure III-9. Day-To-Day Repeatability with Remounting and Exposure to 75°C

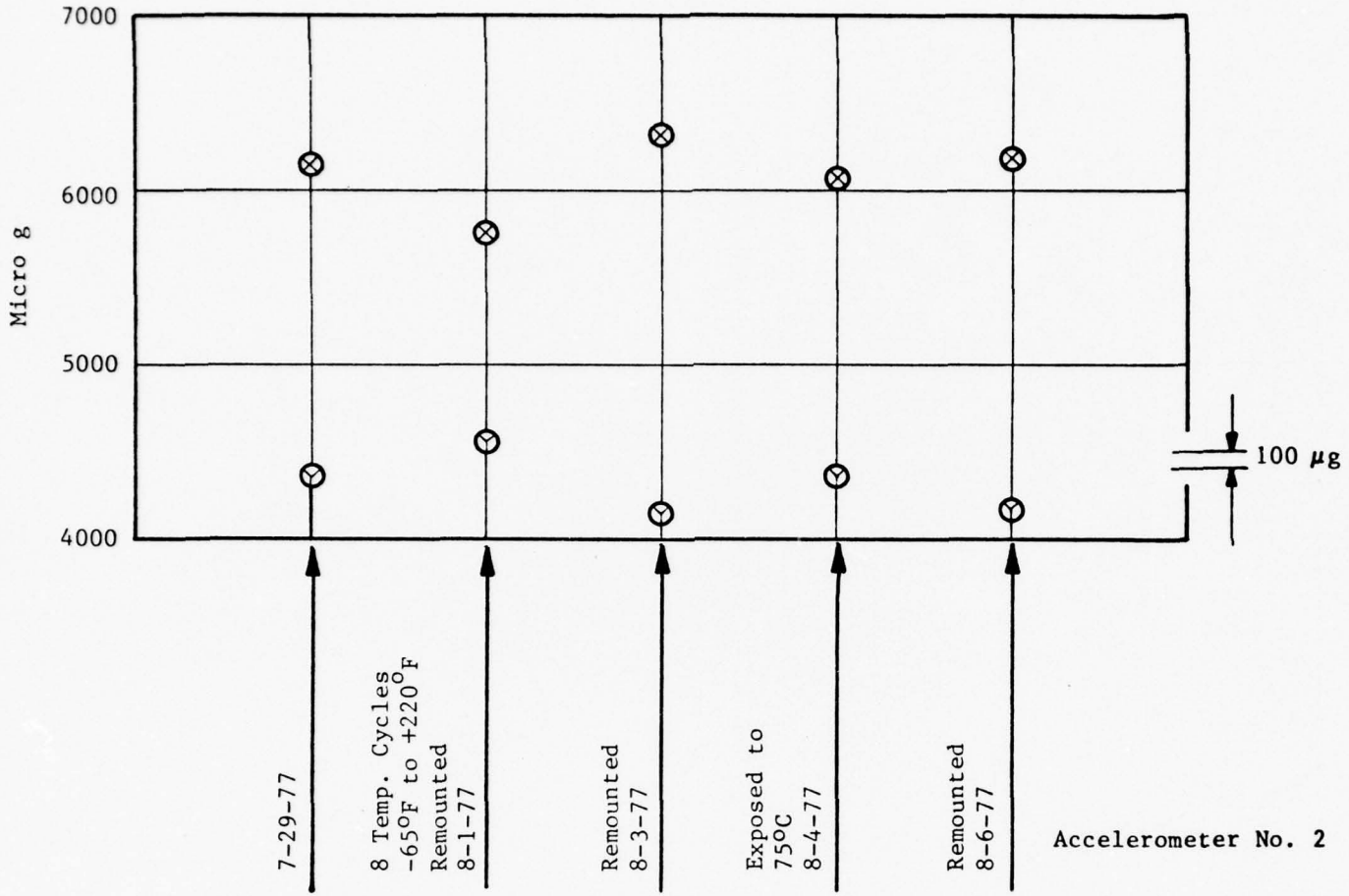

Figure III-10. Day-To-Day Repeatability with Remounting, Exposure to 75°C and Temperature Cycling

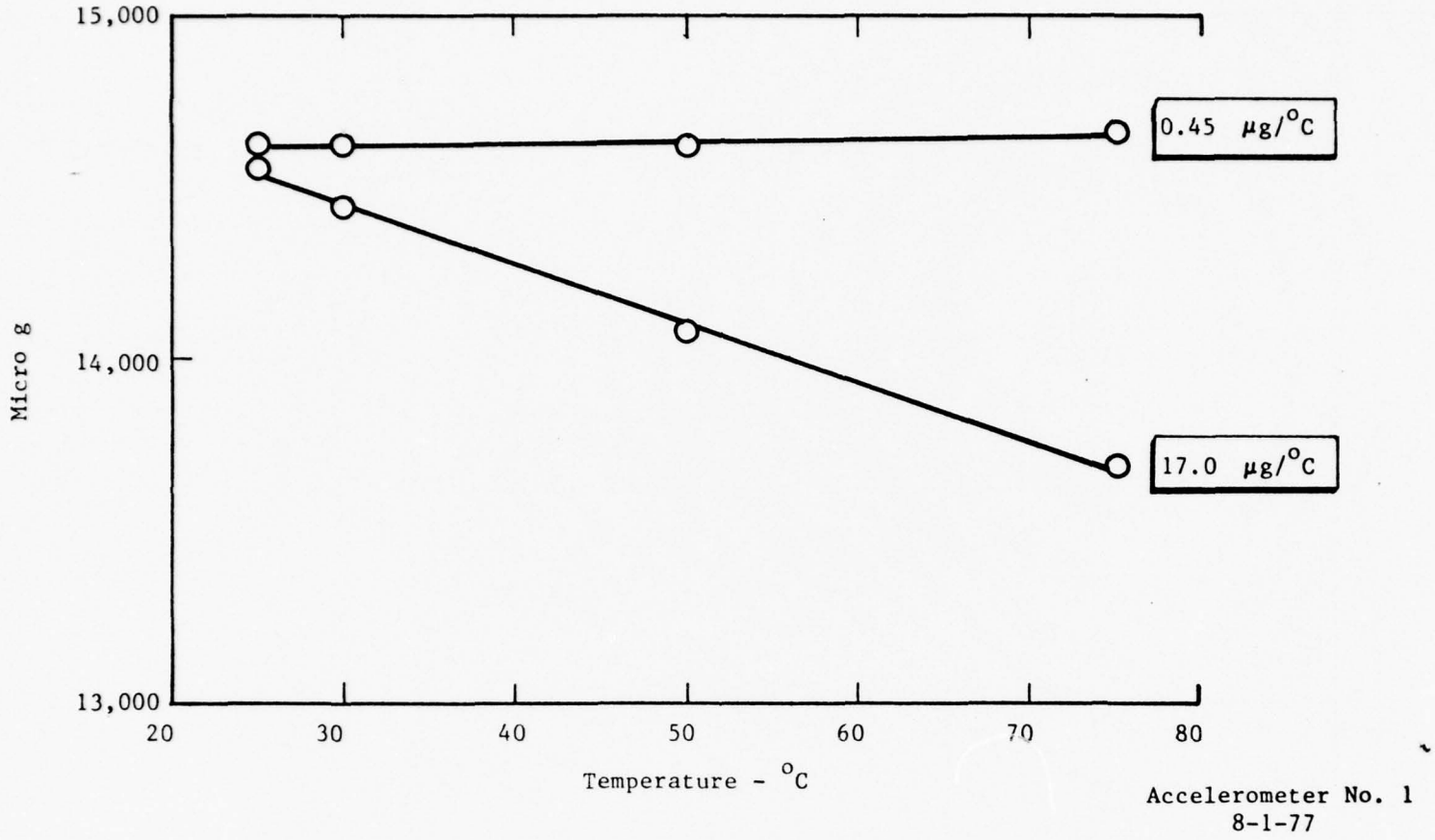

Figure III-11. Uncompensated Bias Temperature Coefficient

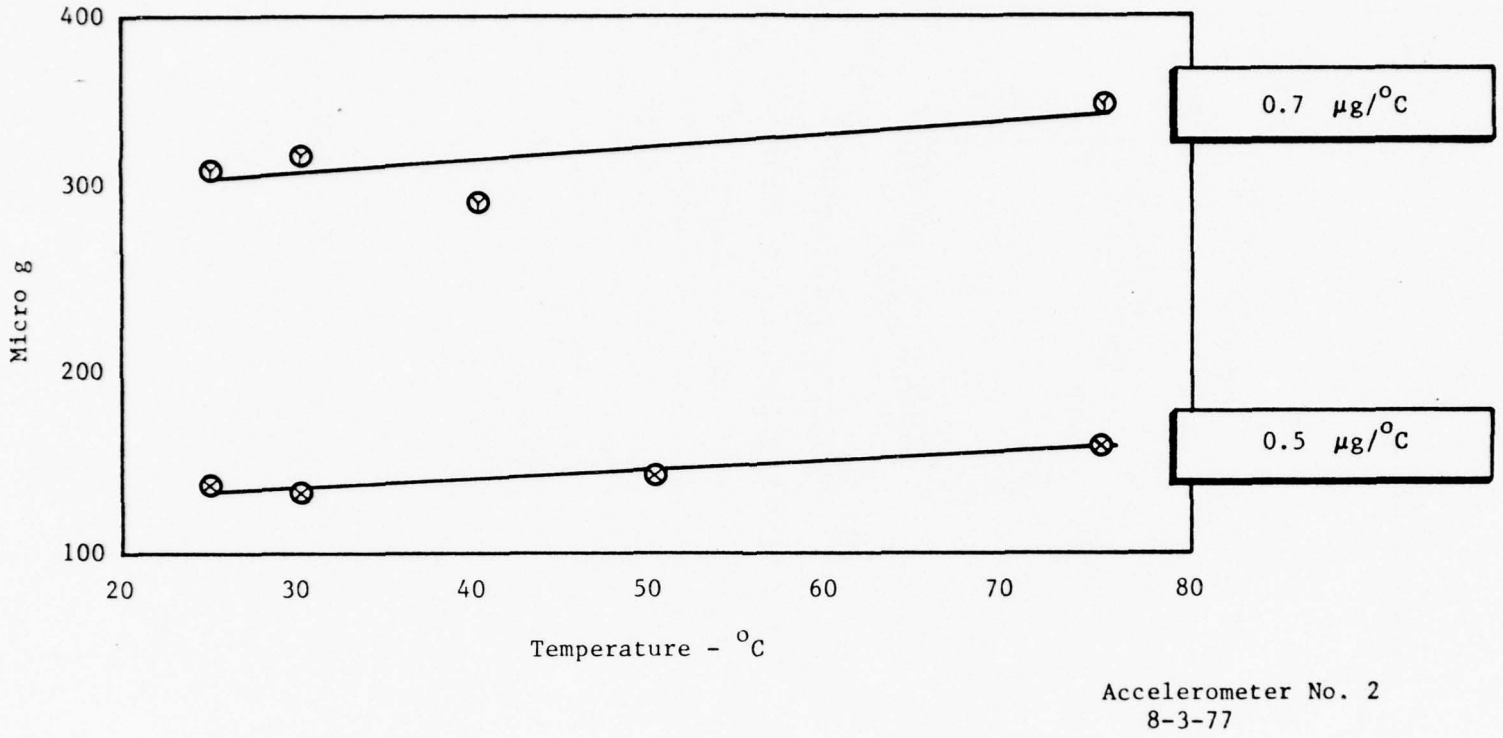

Figure III-12. Uncompensated Bias Temperature Coefficient

TORQUER SCALE FACTOR FOR ACCELEROMETER NO. 1

at 26°C	X-Axis:	0.998850	g/volt
	Y-Axis:	0.969930	g/volt
at 50°C	X-Axis:	0.988628	g/volt
	Y-Axis:	0.960052	g/volt

TEMPERATURE COEFFICIENT OF THE SCALE FACTOR

$$\text{X-Axis } \frac{0.988628 - 0.998850}{(50 - 26)\ 0.99885} = 426 \text{ PPM/}^{\circ}\text{C}$$

$$\text{Y-Axis } \frac{0.960052 - 0.969930}{(50 - 26)\ 0.96993} = 423 \text{ PPM/}^{\circ}\text{C}$$

Figure III-13. Torquer Scale Factor No. 1

TORQUER SCALE FACTOR FOR ACCELEROMETER NO. 2

at 26°C	X-Axis:	0.990208
	Y-Axis:	0.979095
at 50°C	X-Axis:	0.980194
	Y-Axis:	0.969209

TEMPERATURE COEFFICIENT OF THE SCALE FACTOR

$$\text{X-Axis} \quad \frac{0.980194 - 0.990208}{(50 - 26)\ 0.990208} = 421 \text{ PPM/}^{\circ}\text{C}$$

$$\text{Y-Axis} \quad \frac{0.969209 - 0.979095}{(50 - 26)\ 0.979095} = 419 \text{ PPM/}^{\circ}\text{C}$$

Figure III-14. Torquer Scale Factor No. 2

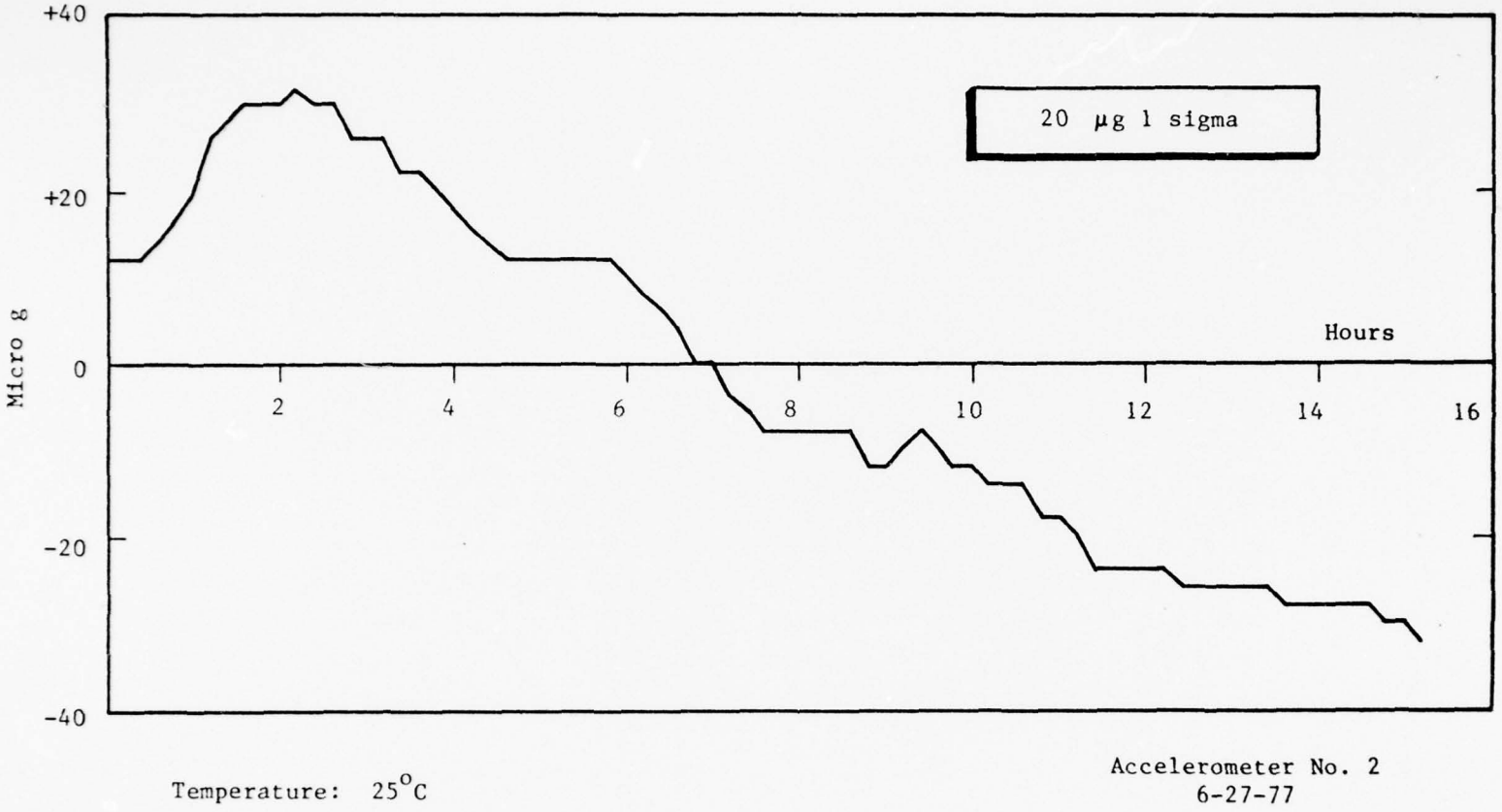

Figure III-15. PAV Long Term Drift

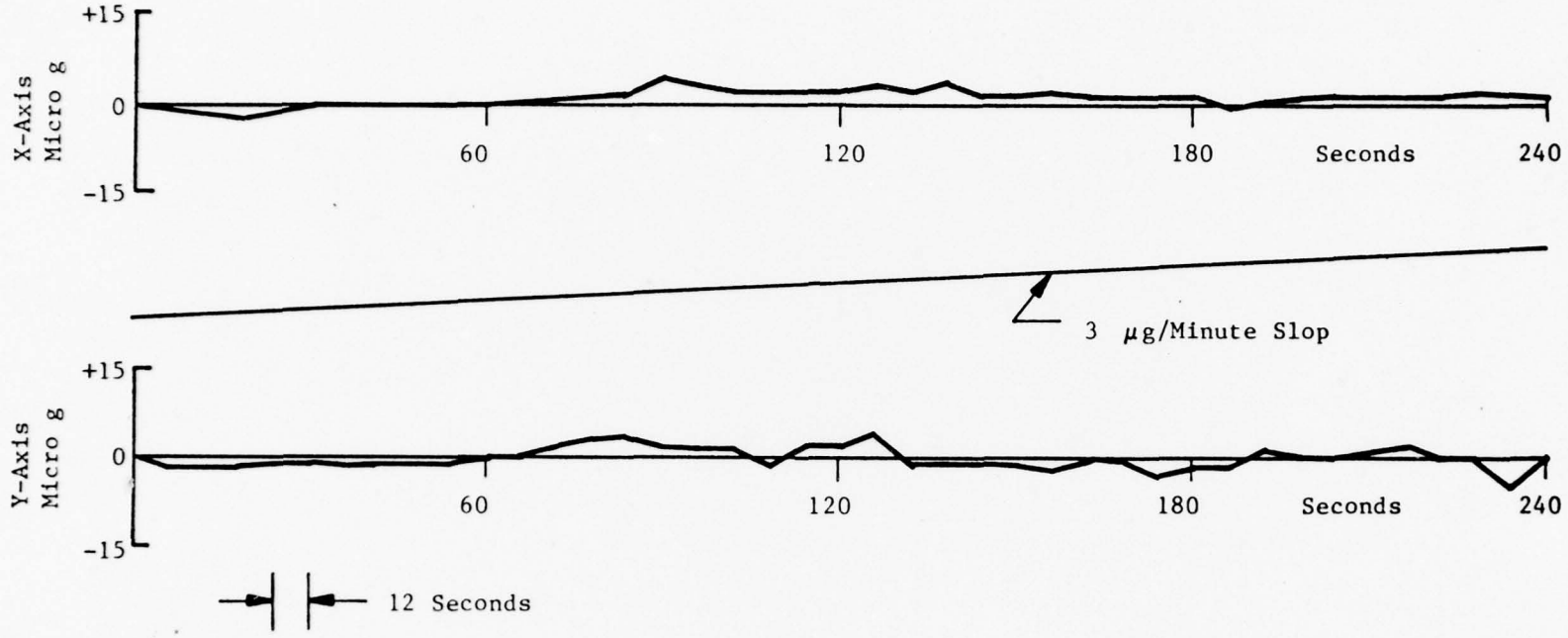

Temperature: 25°C

Accelerometer No. 2
6-29-77

Figure III-16. PAV Short Term Drift Run

IV CONCLUSIONS

The overall accuracy of the accelerometers, and especially the low bias temperature coefficient, illustrates that the design concept is sound. Also of significance is the fact that performance could be predicted accurately prior to an accelerometer being built or tested. This shows that the cause and affect of the component parts on performance can be analyzed, and design modifications made and various configurations established without large expenditures.

It was concluded that the long term bias stability would be improved, expecially after exposure to large temperature variations, by modification of the attachment of the suspension to the case. Variations of this were tried within the allowable funding and time span of the program which did provide positive results. However, it was not possible, nor intended in the scope of the program, to fully optimize the total design.

V RECOMMENDATIONS

The following are the recommendations:

(1) Modify the suspension to case attachment.

(2) Examine methods of adjusting and/or reducing the scale factor temperature sensitivity. It was not intended under this program to consider methods for reducing this parameter, but it will be necessary for accurate systems where no thermal control is required.

(3) Design and develop torquing electronics that give a digital output.

APPENDICES

APPENDIX I

OPEN LOOP MODEL OF A PENDULOUS ACCELEROMETER

In the derivation of this model three coordinate sets are used. These sets are:

$I_i\ P_i\ O_i$ - Accelerometer internal coordinate set

x y z - Pendulum-fixed coordinate set

I P O - Accelerometer case fixed set

The accelerometer internal coordinate set is shown in Figure 1. The O_i axis (output) is coincident with the effective torsional axis of the pendulum suspension system. The pendulous axis, P_i, is orthogonal to and intersects the O_i axis. The P_i axis also passes through the effective center of mass of the pendulum when the sum of all external forces and moments acting on the pendulum and its suspension system is equal to zero. The axis I_i (input) is perpendicular to the plane containing P_i and O_i axes.

For the accelerometer operated in open loop mode, positive acceleration along the input axis causes the pendulum to deflect through positive angle θ about the O_i axis. For θ equal to zero $I_iP_iO_i$ and xyz sets are coincident.

Moments acting on the pendulum about the O_i axis.

It is assumed that the accelerometer is subjected to acceleration and angular rate whose components resolved along the $I_iP_iO_i$ axis set are

$$a_{iI},\ a_{iP},\ a_{iO}$$

and

$$\dot{\phi}_I,\ \dot{\phi}_P,\ \dot{\phi}_O$$

respectively.

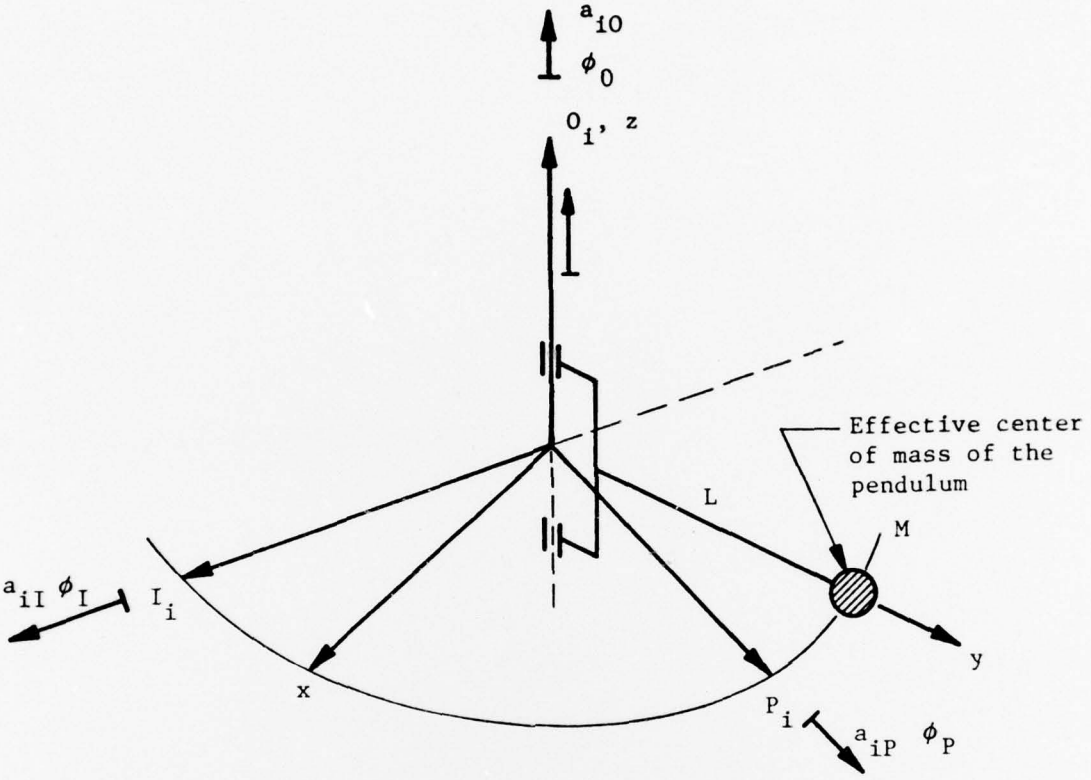

Figure 1. Accelerometer Internal Coordinate Reference Set

The principal of equilibrium of moments applied to the pendulum demands that the resultant of all of these external moments acting on the pendulum must be equal to the inertia moment of the pendulum.

Thus, for the moments about the output axis:

$$T + ML\,(a_{iI} + \ddot{\Theta} a_{iP} + C_{IP}\, a_{iI}\, a_{iP} + C_{IO}\, a_{iI}\, a_{iO} + C_{PO}\, a_{iP}\, a_{iO} + a_B) - D\dot{\Theta} - K\Theta = T_2 \qquad (1)$$

where T is the moment applied to the pendulous mass by the torquer coil and T_2 is the inertia moment of the pendulum stated by equation (5A).

$$T_2 = J_O (\ddot{\phi}_O + \ddot{\Theta}) + (J_P - J_I)\, \dot{\phi}_I\, \dot{\phi}_P + (J_P - J_I)\, (\dot{\phi}_P^2 - \dot{\phi}_I^2)\Theta \qquad (2)$$

Equation (1) may be written

$$T + mL\, a_{iI} + T_E' = J_O\ddot{\Theta} + D\dot{\Theta} + K\Theta \qquad (3)$$

Taking laplace of (3)

$$T_{(S)} + mL\, a_{iI(S)} + T'_{E(S)} = (J_O\, S^2 + DS + K)\ \Theta_{(S)} \qquad (4)$$

T_E' is the error moment and is

$$\begin{aligned} T_E' = mL\, (&\Theta\, a_{iP} \\ &+ C_{IP}\, a_{iI}\, a_{iP} + C_{IO}\, a_{iI}\, a_{iO} + C_{PO}\, a_{iP}\, a_{iO}) \\ &+ a_B \\ &- J_O\ \ddot{\phi}_O \\ &- (J_P - J_I)\ \dot{\phi}_I\, \dot{\phi}_P \\ &- (J_P - J_I)\ (\dot{\phi}_P^2 - \dot{\phi}_I^2)\Theta \end{aligned} \qquad (5)$$

EFFECTS OF MISALIGNMENTS

With reference to Figure 2 we note that the accelerometer internal coordinate set is related to the case fixed set by small angle direction cosine matrix B_C^i, where

$$B_C^i = \begin{bmatrix} 1 & \xi_O & -\xi_P \\ -\xi_O & 1 & 0 \\ \xi_P & 0 & 1 \end{bmatrix} \qquad (6)$$

and

$$\underline{a}^{i} = B_{C}^{i}\,\underline{a}^{C}$$

where $\underline{a}^{i}$ and $\underline{a}^{C}$ is the acceleration vector resolved along internal and case fixed reference sets respectively.

or

$$\begin{bmatrix} a_{iI} \\ a_{iP} \\ a_{iO} \end{bmatrix} = \begin{bmatrix} 1 & \xi_O & -\xi_P \\ -\xi_O & 1 & 0 \\ \xi_P & 0 & 1 \end{bmatrix} \begin{bmatrix} a_{CI} \\ a_{CP} \\ a_{CO} \end{bmatrix}$$

$$\begin{aligned} a_{iI} &= a_{CI} + \xi_O\, a_{CP} - \xi_P\, a_{CO} \\ a_{iP} &= -\xi_O\, a_{CI} + a_{CP} \cong a_{CP} \\ a_{iO} &= \xi_P\, a_{CI} + a_{CO} \cong a_{CO} \end{aligned} \tag{7}$$

Substitute (7) into (3) and (4)

$$T_{(S)} + mL\, a_{CI(S)} + T_{E(S)} = (J_O\, S^2 + DS + K)\, \Phi_{(S)} \tag{8}$$

$$\begin{aligned} T_E = mL\, (&\Phi\, a_{CP} && \text{Vibrapendulous term} \\ &+ C_{IP}\, a_{CI}\, a_{CP} + C_{IO}\, a_{CI}\, a_{CO} && \text{Cross axis sens. terms} \\ &+ C_{PO}\, a_{CP}\, a_{CO}) \\ &+ a_B && \text{Bias term} \\ &- J_O\, \ddot{\phi}_O && \text{Angular acceleration term} \\ &- (J_P - J_I)\, \dot{\phi}_I\, \dot{\phi}_P && \text{Anisoinertia term} \\ &- (J_P - J_I)\, (\dot{\phi}_P^{\,2} - \dot{\phi}_I^{\,2})\, \Phi && \text{Governor effect} \\ &+ \xi_O\, a_{CP} - \xi_P\, a_{CO}) && \text{Misalignment terms} \end{aligned} \tag{9}$$

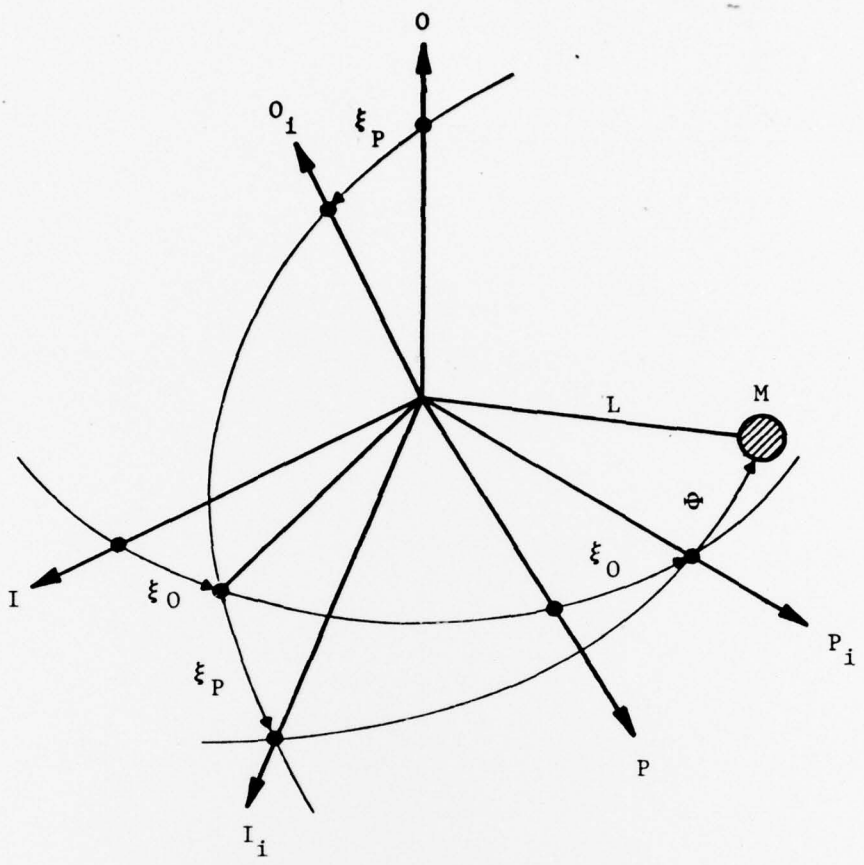

Figure 2. Accelerometer Case and Internal Coordinate Reference Set

From (8)

$$\Theta_{(S)} = \frac{T_{(S)} + mL\, a_{CI(S)} + T_{E(S)}}{J_O S^2 + DS + K} \qquad (10)$$

Equation (10) may be represented in block diagram form as shown in Figure 3.

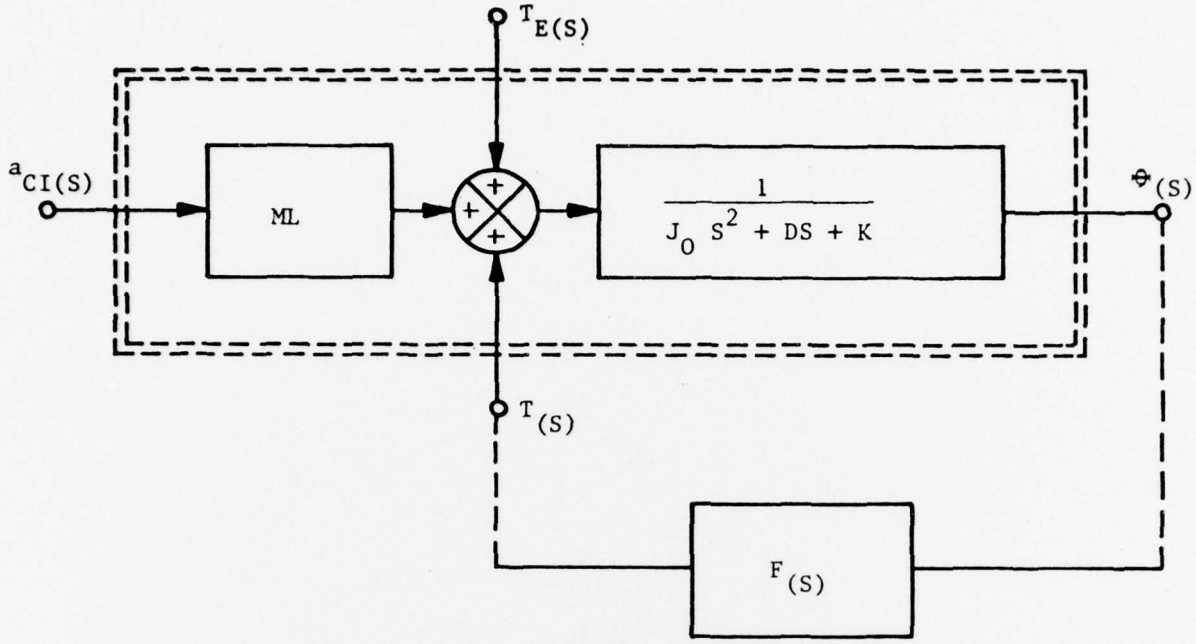

Figure 3. Block Diagram of a Pendulous Accelerometer

Angular velocities of the pendulum resolved along the pendulum fixed axis set xyz. Refer to Figure 1.

$$\omega_x = \dot{\phi}_I + \dot{\phi}_P \Theta$$

$$\omega_y = \dot{\phi}_P - \dot{\phi}_I \Theta$$

$$\omega_z = \dot{\phi}_0 + \dot{\Theta} \qquad (1A)$$

The inertia moment is given by

$$T_2 = \dot{H}_z + \omega_x H_y - \omega_y H_x \qquad (2A)$$

Where

$$H_z = J_0 \omega_z$$

$$H_y = J_P \omega_y$$

$$H_x = J_I \omega_x \qquad (3A)$$

Substitute (1A) into (3A)

$$H_z = J_0 (\dot{\phi}_0 + \dot{\Theta})$$

$$H_y = J_P (\dot{\phi}_P - \dot{\phi}_I \Theta)$$

$$H_z = J_I (\phi_I + \dot{\phi}_P \Theta) \qquad (4A)$$

Substitute (1A) and (4A) into (2A)

$$T_2 = J_0 (\ddot{\phi}_0 + \ddot{\Theta}) + (\dot{\phi}_I + \dot{\phi}_P \Theta) J_P (\dot{\phi}_P - \dot{\phi}_I \Theta) - (\dot{\phi}_P - \dot{\phi}_I \Theta) J_I (\dot{\phi}_I + \dot{\phi}_P \Theta)$$

$$= J_0 (\ddot{\phi}_0 + \ddot{\Theta}) + J_P (\dot{\phi}_I \dot{\phi}_P - \dot{\phi}_I^2 \Theta + \dot{\phi}_P^2 \Theta - \dot{\phi}_P \dot{\phi}_I \Theta^2) - J_I (\dot{\phi}_I \dot{\phi}_P + \dot{\phi}_P^2 \Theta - \dot{\phi}_I^2 \Theta - \dot{\phi}_I \dot{\phi}_P \Theta^2)$$

Neglect

Neglect

$$= J_0 (\ddot{\phi}_0 + \ddot{\Theta}) + (J_P - J_I) \dot{\phi}_I \dot{\phi}_P + (J_P - J_I) (\dot{\phi}_P^2 - \dot{\phi}_I^2) \Theta \qquad (5A)$$

APPENDIX II

DATA REDUCTION EQUATIONS

A.II-1. The following outlines the data reduction equations and their derivation. Also, copies of the actual data sheets used during the program are included.

A.II-2. Two Point Pendulous Axis Vertical (PAV) Test

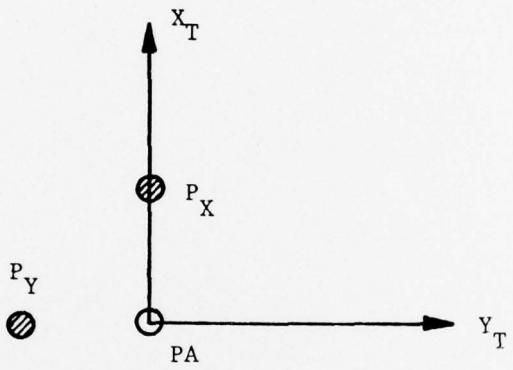

For the pendulous axis up

$$X_1 K_x - \frac{P_y}{P} - B_x = 0 \qquad (1)$$

$$Y_1 K_y - \frac{P_x}{P} - B_y = 0 \qquad (2)$$

For the pendulous axis down

$$X_2 K_x + \frac{P_y}{P} - B_x = 0 \qquad (3)$$

$$Y_2 K_y + \frac{P_x}{P} - B_y = 0 \qquad (4)$$

Equations (1) through (4) represent torques expressed in g's that act on the pendulous mass.

P is the accelerometer pendulosity (5 GM x CM) and P_x and P_y are radial unbalance pendulosities.

From equations (1) through (4) we obtain

$$\frac{P_x}{P} = \frac{(Y_2 - Y_1)\, K_y}{2} \tag{5}$$

$$\frac{P_y}{P} = \frac{(X_2 - X_1)\, K_x}{2} \tag{6}$$

$$B_x = \frac{(X_1 + X_2)\, K_x}{2} \tag{7}$$

$$B_y = \frac{(Y_1 + Y_2)\, K_y}{2} \tag{8}$$

A.II-3. Four Point Pendulous Axis Horizontal (PAH) Test

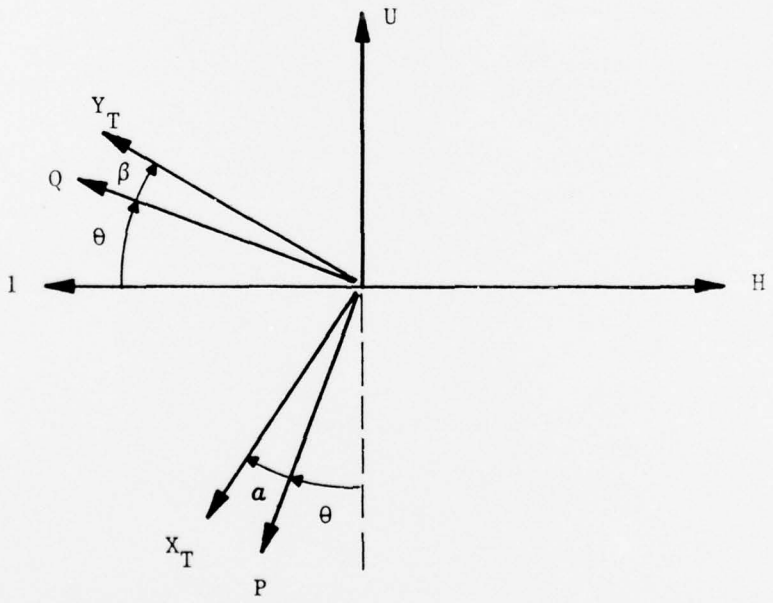

H Horizontal Axis

U Vertical Up Axis

X_T Y_T Torquer Axes

P Q Table Axes

Resolve torques that act on the pendulous mass along P and Q axes.

l is the torque associated with lg.

$$l \sin \theta + XK_x - YK_y\beta - B_P = 0 \tag{9}$$

$$l \cos \theta + YK_y + XK_x\alpha - B_Q = 0 \tag{10}$$

For position 1 $\theta = 0$

$$X_1K_x - Y_1K_y\beta - B_P = 0 \tag{11}$$

$$l + Y_1K_y + X_1K_x\alpha - B_Q = 0 \tag{12}$$

For position 2 $\theta = 90^o$

$$l + X_2K_x - Y_2K_y\beta - B_P = 0 \tag{13}$$

$$Y_2K_y + X_2K_x\alpha - B_Q = 0 \tag{14}$$

For position 3 $\theta = 180^o$

$$X_3K_x - Y_3K_y\beta - B_P = 0 \tag{15}$$

$$-l + Y_3K_y + X_3K_x\alpha - B_Q = 0 \tag{16}$$

For position 4 $\theta = 270^o$

$$-l + X_4K_x - Y_4K_y\beta - B_P = 0 \tag{17}$$

$$Y_4K_y + X_4K_x\alpha - B_Q = 0 \tag{18}$$

Subtract (11) from (15)

$$(X_3 - X_1)\,K_x - (Y_3 - Y_1)\,K_y\beta = 0 \tag{19}$$

Subtract (12) from (16)

$$-2 + (Y_3 - Y_1)\,K_y + (X_3 - X_1)\,K_x\alpha = 0 \tag{20}$$

Subtract (13) from (17)

$$-2 + (X_4 - X_2)\, K_x - (Y_4 - Y_2)\, K_y \beta = 0 \tag{21}$$

Subtract (14) from (18)

$$(Y_4 - Y_2)\, K_y + (X_4 - X_2)\, K_x \alpha = 0 \tag{22}$$

From (19)

$$\beta = \frac{(X_3 - X_1)\, K_x}{(Y_3 - Y_1)\, K_y} \tag{23}$$

From (22)

$$\alpha = -\frac{(Y_4 - Y_2)\, K_y}{(X_4 - X_2)\, K_x} \tag{24}$$

From (20)

$$K_y = \frac{2 - (X_3 - X_1)\, K_x \alpha}{Y_3 - Y_1}$$

$$= \frac{2}{Y_3 - Y_1} - \frac{X_3 - X_1}{Y_3 - Y_1} K_x \alpha$$

Substitute from (24)

$$K_y = \frac{2}{Y_3 - Y_1} - \frac{X_3 - X_1}{Y_3 - Y_1} K_x \frac{Y_4 - Y_2}{X_4 - X_2} \frac{K_y}{K_x}$$

$$K_y \left[1 + \frac{(X_3 - X_1)\,(Y_4 - Y_2)}{(Y_3 - Y_1)\,(X_4 - X_2)}\right] = \frac{2}{Y_3 - Y_1}$$

$$K_y = \frac{2}{Y_3 - Y_1} \left[1 + \frac{(X_3 - X_1)\,(Y_4 - Y_2)}{(Y_3 - Y_1)\,(X_4 - X_2)}\right] \tag{25}$$

From (21)

$$K_x = \frac{2 + (Y_4 - Y_2)\, K_y \beta}{X_4 - X_2}$$

$$= \frac{2}{X_4 - X_2} + \frac{Y_4 - Y_2}{X_4 - X_2}\, K_y \beta$$

Substitute from (23)

$$K_x = \frac{2}{X_4 - X_2} + \frac{Y_4 - Y_2}{X_4 - X_2}\, K_y \, \frac{X_3 - X_1}{Y_3 - Y_1}\, \frac{K_x}{K_y}$$

$$K_x \left[1 - \frac{(Y_4 - Y_2)\,(X_3 - X_1)}{(X_4 - X_2)\,(Y_3 - Y_1)} \right] = \frac{2}{X_4 - X_2}$$

$$K_x = \frac{2}{X_4 - X_2} \left[1 - \frac{(Y_4 - Y_2)\,(X_3 - X_1)}{(X_4 - X_2)\,(Y_3 - Y_1)} \right]^{-1} \tag{26}$$

$$\frac{K_x}{K_y} \cong \frac{Y_3 - Y_1}{X_4 - X_2} \tag{27}$$

Substitute (27) into (23) and (24)

$$\beta = \frac{X_3 - X_1}{\cancel{Y_3 - Y_1}} \times \frac{\cancel{Y_3 - Y_1}}{X_4 - X_2} = \frac{X_3 - X_1}{X_4 - X_2} \tag{28}$$

$$\alpha = \frac{Y_4 - Y_2}{\cancel{X_4 - X_2}} \times \frac{\cancel{X_4 - X_2}}{Y_3 - Y_1} = \frac{Y_4 - Y_2}{Y_3 - Y_1} \tag{29}$$

Substitute (28) and (29) into (25) and (26)

$$K_y = \frac{2}{Y_3 - Y_1} \left[1 - \alpha\beta \right]^{-1} \tag{30}$$

$$K_x = \frac{2}{X_4 - X_2} \left[1 + \alpha\beta \right]^{-1} \tag{31}$$